Particle statistics and lossy dynamics of ultracold atoms in optical lattices

J. Yago Malo,[1] E. P. L. van Nieuwenburg,[2,3] M. H. Fischer,[2] and A. J. Daley[1]
[1]*Department of Physics and SUPA, University of Strathclyde, Glasgow G4 0NG, Scotland, United Kingdom*
[2]*Institute for Theoretical Physics, ETH Zurich, 8093 Zurich, Switzerland*
[3]*Institute for Quantum Information and Matter, Caltech, Pasadena, California 91125, USA*

(Received 12 September 2017; published 21 May 2018)

Experimental control over ultracold quantum gases has made it possible to investigate low-dimensional systems of both bosonic and fermionic atoms. In closed one-dimensional systems there are many similarities in the dynamics of local quantities for spinless fermions and strongly interacting "hard-core" bosons, which on a lattice can be formalized via a Jordan-Wigner transformation. In this study, we analyze the similarities and differences for spinless fermions and hard-core bosons on a lattice in the presence of particle loss. The removal of a single fermion causes differences in local quantities compared with the bosonic case because of the different particle exchange symmetry in the two cases. We identify deterministic and probabilistic signatures of these dynamics in terms of local particle density, which could be measured in ongoing experiments with quantum gas microscopes.

DOI: 10.1103/PhysRevA.97.053614

I. INTRODUCTION

In the past few years, there has been rapid progress in the characterization and control of dissipative dynamics for ultracold atoms in optical lattices. While these systems are most known for the possibility to engineer Hamiltonians for strongly interacting systems towards quantum simulation purposes, [1,2], the same level of microscopic understanding, in which models can be derived from first principles under well-controlled approximations, is also available for most of the dominant forms of dissipation that occur naturally in experiments. This applies, in particular, to our understanding of incoherent light scattering and the resulting dephasing of the many-body state [3,4] and to our treatment of atom loss [5]. Studying these sources of dissipation is of importance well beyond gaining a better understanding of experimental imperfections: it allows for the use of dissipation (1) in probing many-body states and their dynamics [6,7], (2) in the controlled preparation of interesting many-body states [6,8], and (3) in understanding how signatures of fundamental effects from closed systems (e.g., many-body localization) survive in the presence of coupling to an environment [9–13].

In this work, we explore how the differences between many-body states of hard-core bosons (HCBs) and spinless fermions confined to move in one dimension can be probed using particle loss. In one dimension, where strongly interacting bosons cannot pass each other, there are strong formal similarities between HCBs and spinless fermions [14]. These regimes have been realized in experiments with cold bosonic atoms in strongly confined one-dimensional (1D) tubes [15], and in lattices [16,17], and the consequences can be seen clearly, even for just two atoms, in quantum gas microscope experiments [18]. For particles moving on a lattice, this similarity can be formalized via a Jordan-Wigner transformation to spin operators [19], where we see that for local models, the energy eigenvalues will be identical, and local correlations—both for the eigenstates and for out-of-equilibrium dynamics induced by changing local trap quantities—will be equal as well. However, single-particle loss can generate differences in local quantities due to the different exchange symmetries in the many-body wave function. These differences manifest themselves in local density distributions, which are accessible with current experimental techniques in quantum gas microscopes [20–25].

Making use of symmetries in tensor-network-based numerical methods, we calculate the dynamics of example systems for typical experimental sizes and parameter scales in the presence of loss. The efficient simulation of such systems requires the proper inclusion of symmetries in these numerical methods in order to account for the loss process in an affordable manner. We first study the loss process as a deterministic event and then employ a quantum trajectory approach [26–28] to determine features of bosons and fermions that survive stochastically occurring loss events.

The rest of the paper is structured as follows. In Sec. II we discuss the theoretical model for fermions and bosons confined in one dimension subject to dissipation. In Sec. III we highlight the differences we expect to observe between the different types of particle statistics in the event of a loss, and in Sec. IV we describe the numerical approach that allows for the computationally efficient simulation of a system subject to this kind of dissipation. In Sec. V we then analyze the dynamics following losses that occur at deterministic times and locations, identifying accessible parameter regimes where the differences between HCBs and spinless fermions are significant and could be engineered and observed using quantum gas microscopes [29–31]. In Sec. VI we study which of those features identified in Sec. V survive under stochastic losses and which of them vanish when the losses occur randomly, providing local and spatially averaged quantities that can be obtained through density measurements. Finally, in Sec. VII we discuss our findings.

II. MODEL: FERMIONS AND HARD-CORE BOSONS IN THE PRESENCE OF LOCAL PARTICLE LOSS

In this section, we introduce a model for particle loss in spinless fermions or hard-core bosons confined to move along one direction of an optical lattice (and tightly confined in the other two directions).

For fermions in the lowest Bloch band of the optical lattice, the system is well described by a tight-binding Hamiltonian($\hbar \equiv 1$),

$$\hat{H} = -J \sum_{i}^{M-1} (\hat{a}_i^\dagger \hat{a}_{i+1} + \text{H.c.}), \tag{1}$$

where i indicates the lattice site, with lattice length M, the operator $\hat{a}_i^{(\dagger)}$ annihilates (creates) a fermionic particle on the site i where $\hat{n}_{a,i} = \hat{a}_i^\dagger \hat{a}_i \in [0,1]$ is the fermionic number operator of the site $i \in [1,M]$, where M is the lattice system size, and J is the tunneling amplitude in the lattice. The fermionic operators obey the usual anticommutation rules, $\{\hat{a}_i^{(\dagger)}, \hat{a}_j^{(\dagger)}\} = 0$; $\{\hat{a}_i, \hat{a}_j^\dagger\} = \delta_{i,j}$.

An analogous model can be considered for the case of hard-core bosons, for which the Hamiltonian can be seen as a limiting case of the Bose-Hubbard Hamiltonian [32], and is given by

$$\hat{H} = -J \sum_{i}^{M-1} (\hat{b}_i^\dagger \hat{b}_{i+1} + \text{H.c.}), \;\; \hat{b}_1^2 \equiv 0, \tag{2}$$

where the operator $\hat{b}_i^{(\dagger)}$ annihilates (creates) a bosonic particle on the site i and $\hat{n}_{b,i} = \hat{b}_i^\dagger \hat{b}_i \in [0,1]$ is the bosonic number operator for the site i. In contrast to the fermionic case, the bosonic creation and annihilation operators obey usual commutation rules, $[\hat{b}_i^{(\dagger)}, \hat{b}_j^{(\dagger)}] = 0$; $[\hat{b}_i, \hat{b}_j^\dagger] = \delta_{i,j}$.

We can describe the dissipative dynamics of such systems in the presence of particle loss via a master equation for the system density operator ρ_{tot}. The master equation arises on a microscopic level because in these atomic-physics systems we can usually make a Born-Markov approximation, justified by the existence of a single dominant frequency for each process (given by the energy of the lost atom for single-particle loss, and by the photon frequency for dephasing due to light scattering [28]). The resulting master equation is given by

$$\frac{d\rho}{dt} = -i[\hat{H}, \rho] - \frac{1}{2} \sum_{m,\alpha}^{M} \gamma_{\alpha,m} (\hat{J}_{\alpha,m}^\dagger \hat{J}_{\alpha,m} \rho + \rho \hat{J}_{\alpha,m}^\dagger \hat{J}_{\alpha,m} - 2\hat{J}_{\alpha,m} \rho \hat{J}_{\alpha,m}^\dagger), \tag{3}$$

where $\alpha \in \{l,d\}$ is an index summing over the separate terms for loss and dephasing, $\hat{J}_{l,m} = \hat{a}_m(\hat{b}_m)$ represents the loss of a fermion (boson) on site m, $\hat{J}_{d,m} = \hat{n}_{a,m}(\hat{n}_{b,m})$ describes the dephasing process, and $\gamma_{l/d,m}$ is the decay amplitude for the mth dissipation channel that will be different for dephasing and loss processes. The inclusion of dephasing, which is naturally present in experimental realizations due to light scattering [3,4,9,33], will allow us to test whether any differences between spinless fermions and bosons are diminished by this form of dissipation. Numerical solutions to the evolution of the system will be discussed in subsequent sections.

Figure 1 shows a schematic view of the density profiles after a deterministic loss event in the middle site at $t = 0$, beginning from an initial product state with one atom on every lattice site. Because of the simple initial state and the single loss process, the density distributions for bosons and fermions as a function of time are identical, i.e., the normalized difference,

$$\Delta n_i = \frac{n_i^b - n_i^f}{n_i^b + n_i^f}, \tag{4}$$

where $n_i^b = \langle \hat{n}_{b,i} \rangle$ and $n_i^f = \langle \hat{n}_{a,i} \rangle$, is zero in this case. For the case of vanishing densities $n_i^b + n_i^f = 0$, which happens only in certain initial states, we set the normalized difference to $\Delta n_i = 0$. In analyzing different parameter regimes and identifying differences between HCBs and spinless fermions, we focus particularly on this quantity in the following sections.

III. DIFFERENCES BETWEEN FERMIONS AND BOSONS IN THE PRESENCE OF LOSS

Bosonic and fermionic atoms will behave differently in the presence of dissipation as a result of the difference in the sign of the wave function under exchange of particles. One way to see this is to use a Jordan-Wigner transformation to map each of these cases to spin operators [19]. A single-species model for hard-core bosons can be directly rewritten as an equivalent spin-1/2 model, with the spin states associated with each lattice site denoting presence ($|\uparrow\rangle$) or absence ($|\downarrow\rangle$) of a particle on that site. Because bosons commute, the mapping between particle annihilation operators and spin lowering operators $\hat{\sigma}_l^-$ is a direct replacement, $\hat{b}_l \to \hat{\sigma}_l^-$. However, the same mapping for fermions requires a sign determined by a string operator in order to account for anticommutation of the annihilation operators with all other operators present in the state description,

$$\hat{a}_l \to (-1)^{\sum_{i<l} \hat{n}_{a,i}} \hat{\sigma}_l^-. \tag{5}$$

It is clear that a loss event can thus affect the many-body state differently for fermions and for hard-core bosons. Our goal here is to identify whether there are differences that can be extracted solely from the local density distribution, $\hat{n}_{a/b,l}$, which translates the same way into spin operators for bosons and fermions under a Jordan-Wigner transformation, $\hat{n}_{a/b,l} \to \hat{\sigma}_l^+ \hat{\sigma}_l^-$. Indeed, for unitary dynamics involving only onsite and nearest-neighbor terms, the two cases, of spinless fermions and HCBs, are identical as all of the signs vanish.

The vanishing of these phases for fermions after the transformation can be easily understood if we consider that they arise in the first place due to the commutation of the annihilation operators with the rest of the operators describing the state of the system. The local density is proportional to a product of two operators $\hat{n}_{a,i} = \hat{a}_l^\dagger \hat{a}_l$, thus any phase that arises from the commutation will cancel and $\hat{n}_{a,i} = \hat{\sigma}_l^+ \hat{\sigma}_l^-$. Similarly, if we consider terms that include only first-neighbor tunneling $\hat{a}_l^\dagger \hat{a}_{l\pm1}$ all signs will disappear, and so under local perturbations, the dynamics are identical for both species. Physically, this arises because these local operators cannot (for spinless fermions or HCBs) exchange two particles that are present on different sites. However, in the presence of loss, there is an additional sign from the commutation of the operator

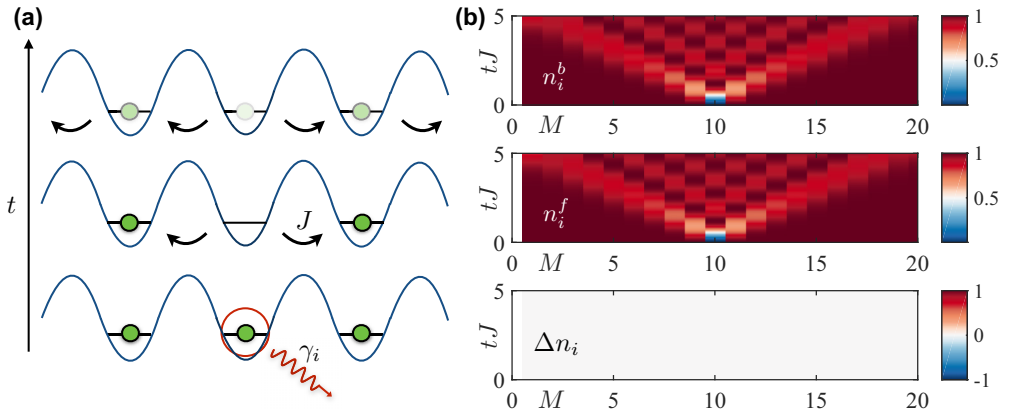

FIG. 1. (a) Diagram of a loss event in an optical lattice on site i with probability γ_i. The density hole created will propagate through normal tunneling processes and will delocalize over time. (b) Evolution of the particle density for bosons $\hat{n}_i^b$, fermions $\hat{n}_i^f$, and the normalized difference of these, Δn_i, as a function of time. In this case, loss occurs on site $i = 10$ on a lattice with $M = 20$ from an initial product state with a single particle on each site, so a single sign is applied to the fermionic wave function and both profiles remain identical: $\Delta n_i = 0$.

to the respective site. This also implies that when expressed in terms of spin operators the loss operator is in principle nonlocal for fermions due to their anticommutation rules; see Eq. (5).

IV. NUMERICAL METHODS AND THE RELEVANCE OF SYSTEM SYMMETRIES

In order to determine the dynamics for up to tens of lattice sites (which correspond to current experiments [20–25]), we make use of tensor-network methods [34–36]. These methods provide us with efficient tools to compute the time evolution of both closed and open 1D many-body systems through the time-evolving block decimation (TEBD) algorithm [37]. In particular, open dynamics have been described through tensor networks by mapping the density operator ρ to a matrix product operator (MPO) [38,39]. Alternatively, the system evolution can be computed using a quantum trajectory approach [28] where we can map the density operator dynamics to a stochastic sampling of pure-state evolutions in the form of matrix product states.

When we consider the case of fermionic losses, the string operator $\hat{N}_{<k} = (-1)^{\sum_{i<k}\hat{n}_{a,i}}$ is an expensive operator to compute in terms of matrix product states, because it is a highly nonlocal term and lacks a simple representation as an MPO. However, as shown recently [13], this operator can be efficiently applied if we split our state representation into parity-conserving sectors. In a similar manner, we will benefit from making use of number-conserving sectors [40,41], which optimize time evolution calculations for pure states implementing quantum-trajectories techniques for the master equation [28].

In this particular case, we structure the matrix product state in such a way that the storage scheme for the local tensor A^{d_i} (with maximum bond dimension D) for site i with local dimension d_i [in our case $d_i = \dim(n_i) = 2$] groups together the states that correspond to every possible population quantum number to the left of site i. In this way, the string operator reduces to a trivial value $N_{<k} = \pm 1$ depending on a number that we store for every state in every site. As a result, the application of an annihilation operator, representing a loss in the lattice, becomes the application of a local operator multiplied by a known phase.

Note that all the other terms appearing in the dynamics [Eq. (1) and Eq. (3)], in both the unitary and the dissipative part, are either proportional to $\hat{n}_{a,i} = \hat{a}_i^\dagger \hat{a}_i$ or proportional to $\hat{a}_i^\dagger \hat{a}_{i\pm1}$, with all string operators evaluating to one as discussed in Sec. III. Thus, the only nonlocal phase arises from the loss term that we have already adapted. As a result, we can apply standard TEBD algorithms to compute the time evolution and study the dissipative dynamics through quantum trajectories efficiently as all our terms become local.

Below we will first use these techniques to compute the dynamics resulting from loss at a particular site and a particular time. We then follow this by simulating a master equation that describes loss processes that occur at random during the dynamics.

V. DETERMINISTIC LOSSES

In this section we study the dynamics of the system when we induce the loss of a particle starting from a particular initial state. This could be achieved in a quantum gas microscope using single-site addressing (freezing the state by rapidly increasing the lattice depth, changing the internal state, and removing the resulting atoms [30]) or by making use of addressing with an electron beam [31].

Outside of the loss events, we compute the unitary evolution of spinless fermions and hard-core bosons governed by the Hamiltonians in Eqs. (1) and (2). We first consider the atoms to be in a product state and induce a loss at $t = 0$ on site $M_0 = M/2$. A second loss event is then induced at a chosen time $t = \tau_0$ on site $M_0 - \delta_M$, with δ_M a chosen lattice distance. We consider different filling factors $n_0 = N_0/M$, where N_0 is the initial number of particles and M is the number of lattice sites. In particular, we will start both with a configuration consisting of a single atom per site ($n_0 = 1$) and a charge density wave state, with only odd sites occupied initially ($n_0 = 0.5$).

In Fig. 2 we present the difference in density distribution Δn_i. We observe that the dynamical evolution of the density of hard-core bosons and fermions is identical up to the point of the

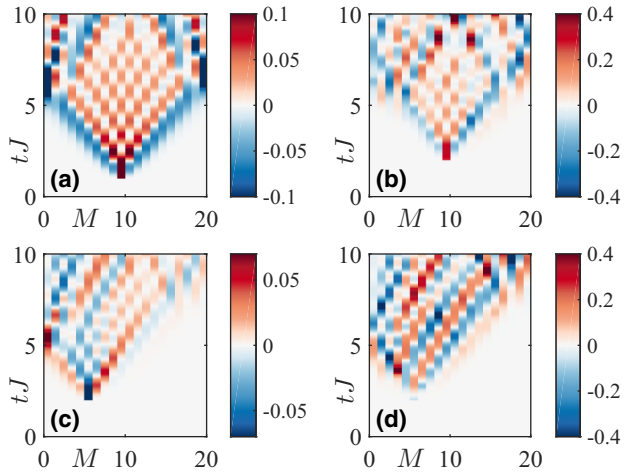

FIG. 2. (a) Evolution of the difference in density distribution Δn_i for a system with $M = 20$, $n_0 = 1$, $D = 100$, $dt = 0.001$, $J = 1$, $\tau_0 = 1$, $\delta_M = 0$. (b) Same as (a) with $\tau_0 = 2$ and $n_0 = 0.5$. (c) Same as (a) with $\tau_0 = 2$ and $\delta_M = 4$. (d) Same as (a) with $\tau_0 = 2$, $n_0 = 0.5$ and $\delta_M = 4$. These calculations are performed beginning from a product state with the corresponding densities indicated above: a single particle on each lattice site ($n_0 = 1$) or every odd site ($n_0 = 0.5$).

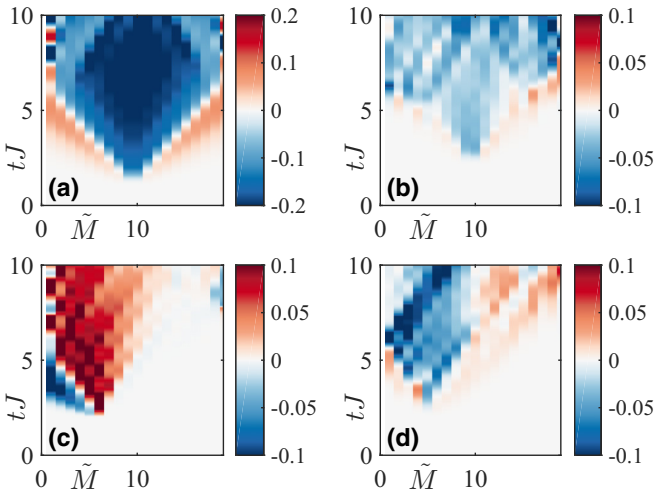

FIG. 3. (a) Evolution of the weighted difference in the entanglement entropy ΔS at every lattice bipartition $\tilde{M} \in [1, M-1]$ for a system with $M = 20$, $n_0 = 1$, $D = 100$, $dt = 0.001$, $J = 1$, $\tau_0 = 1$, $\delta_M = 0$. (b) Same as (a) with $\tau_0 = 2$ and $n_0 = 0.5$. (c) Same as (a) with $\tau_0 = 2$ and $\delta_M = 4$. (d) Same as (a) with $\tau_0 = 2$, $n_0 = 0.5$ and $\delta_M = 4$. These calculations are performed beginning from a product state with the corresponding densities indicated above: a single particle on each lattice site ($n_0 = 1$) or every odd site ($n_0 = 0.5$).

second loss event. This occurs because the initial product state results in a single phase being applied to the whole fermionic state $N_{<M/2} = \pm 1$, as was shown in Fig. 1. However, when the second loss occurs, the delocalization of the initial hole results in a superposition of different numbers of particles to the left of any given site, and so the effect of the phase is nontrivial. As a result, the densities of HCBs and spinless fermions start to differ in a well-defined light cone in a ballistic manner. This is reminiscent of the spreading of correlation functions we expect in this system [42]. In the unit-filling regime [Figs. 2(a) and 2(c)], we observe that only losses occurring close to the region where the first one occurred ($\delta_M \sim 0$), i.e., where the population is not still deeply in the unit-filling Mott phase, lead to a significant difference between bosons and fermions, as it is only in this case that the effects of the string operator are nontrivial. The fact that differences appear only after the second loss in the unit-filling regime can also be understood from the perspective of a particle-hole mapping, since the particle statistics are not relevant until a second particle (hole) has appeared in the system.

In the case of half-filling [Figs. 2(b) and 2(d)], as the particles are allowed to quickly delocalize, the difference is greater in magnitude and the relevance of the position where the second loss occur disappears. In Appendix A we discuss the possible dependence of this profiles with the system size and the density evolution before the first loss.

In Fig. 3 we present the weighted difference in the entanglement entropy $\Delta S = \frac{S^b_{vN} - S^f_{vN}}{S^b_{vN} + S^f_{vN}}$, where $S^{b/f}_{vN} = -\mathrm{tr}(\rho^{b/f} \ln \rho^{b/f})$ at every bipartition of both the bosonic and fermionic systems. This is another indicator of the differences in the dynamics and can also be measured directly in quantum gas microscope experiments for both fermions and HCBs [43–45]. After the losses occur we observe regions with higher entropy for the bosonic case as the nonlocal phase associated with the fermionic loss permits a faster spreading of the entanglement along the system. Note that now lattice configurations away from unit filling [compare Figs. 3(a) and 3(b)] exhibit smaller differences between fermions and bosons. This is due to the fact that the higher mobility in the lattice contributes to overall higher values of S_{vN} for both species, and we are representing normalized differences. Similar to the case of the density, losses that occur near the boundary of the lattice [Figs. 3(c) and 3(d)] lead to a smaller observable difference as the fermionic state is closer to a product state.

VI. NONDETERMINISTIC LOSSES

While these differences between HCBs and spinless fermions can be probed directly in experiments by inducing losses at particular lattice sites and times, it is important also to ask whether the difference is directly observable when losses occur at random, for example, via collisions with background gas or photon scattering bursts [9]. In experiments, we also typically deal with two other elements that we have not included up to now. First, we usually encounter some level of dephasing due to light scattering. In addition, at finite interaction strengths between bosons, a nearest-neighbor interaction term arises in second-order perturbation theory, which we model by considering interactions of the form $\sum_{\langle ij \rangle} V \hat{n}_i \hat{n}_j$ with $V \propto J^2/U$ and U the onsite interaction that we will consider as finite when including this term. We note that this can also arise, e.g., due to direct dipole-dipole interactions between atoms on neighboring lattice sites [46], which allow for larger V values, including up to $V \approx J$, which we will use in some of the calculations below.

To properly investigate the effects of the former in typical experiments, we compute the dissipative dynamics in the

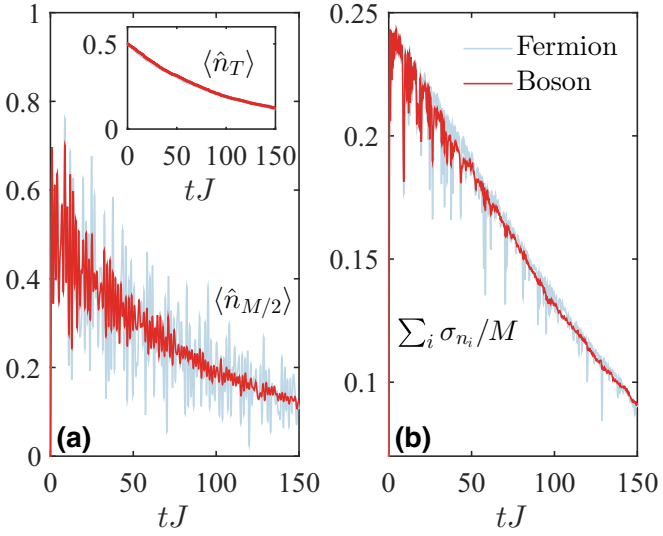

FIG. 4. (a) Comparison of bosonic and fermionic evolution of the middle site density $\langle \hat{n}_{M/2} \rangle$ for a system with $M = 16$, $n_0 = 0.5$, $J = 1$, $\gamma_l = 0.01$, $\gamma_d = 0$; numerical parameters are $dt = 0.001$ and $D = 200$. The inset shows the total particle number $\langle \hat{n}_T \rangle$ to provide some guidance over the evolution of the total occupation in the lattice as losses occur. (b) Same as (a) for the normalized total density fluctuations $\sum_i \sigma_{n_i}/M$. These calculations are performed beginning from a charge density wave at half-filling, with a particle on each even-numbered site.

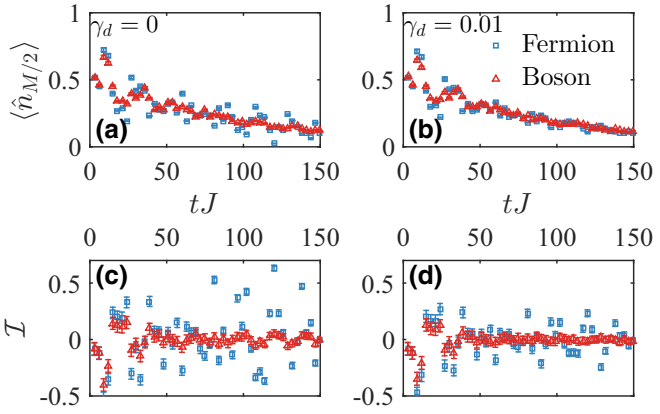

FIG. 5. (a) Comparison of bosonic and fermionic evolution of the middle site density $\langle \hat{n}_{M/2} \rangle$ for a system with $M = 16$, $n_0 = 0.5$, $J = 1$, $dt = 0.001$, $\gamma_l = 0.01$, $\gamma_d = 0$. (b) Same as (a) with $\gamma_d = 0.01$. (c) Comparison of bosonic and fermionic evolution of the imbalance $\mathcal{I}$ with same parameters as (a). (d) Same as (c) with $\gamma_d = 0.01$. These calculations are performed beginning from a charge density wave at half-filling, with a particle on each odd-numbered site. Note that these functions are rapidly oscillating, and that each point represents a snapshot of the values on a regularly spaced grid in time.

presence of both losses (with amplitude γ_l) and dephasing (with amplitude γ_d) for the same initial configurations provided in the deterministic case. We focus our interest again on quantities related to local densities that can be measured in quantum gas microscopes and that would be identical for HCBs and spinless fermions in the absence of losses. The closed system scenario and the comparison with the presented results is discussed in depth in Appendix C.

In Fig. 4 we consider the evolution of local densities, spatially averaged density fluctuations and total particle numbers for both fermions and bosons. Figure 4(a) shows the local density on the central site $\langle \hat{n}_{M/2} \rangle$, where we observe measurable differences between fermions and bosons persisting over time. Specifically, we observe that local densities experience significantly larger fluctuations in time in the fermionic case. This occurs despite the fact that the spatially averaged value which is $\langle \hat{n}_T \rangle$ coincides [see inset Fig. 4(a)]. The total number of particles $\langle \hat{n}_T \rangle$ is the same since both HCBs and fermions are subject to the same single-particle loss rate γ_l. In Fig. 4(b) we compute the lattice-averaged fluctuations $\sum_i \sigma_{n_i} = \sum_i (\langle \hat{n}_i^2 \rangle - \langle \hat{n}_i \rangle^2)$. We observe again higher fluctuations in the fermionic case. However, the difference now is smaller than in the case of local densities. Moreover, the fluctuations of the fermions occur for only short times and might be difficult to resolve in experiments. These sudden drops in the on-site density fluctuations are associated with increases in the CDW correlations that occur due to boundary effects and hence are also size-dependent. Therefore, we must be careful to check whether this difference is measurable in experiments. In Appendix B we show that this is the case, by considering a worst-case scenario of shifted snapshots in time taken on a randomised time grid. There we observe that the difference between HCBs and spinless fermions is still measurable.

From the previous discussion one could conclude that the lattice averaging makes the distinction between HCBs and fermions rather complicated. However, not all the global quantities suffer from the averaging. To look at this further, we consider the total odd-even site density imbalance,

$$\mathcal{I} = \frac{n^o - n^e}{n^o + n^e}, \tag{6}$$

where $n^{o/e} = \sum_{i \in \text{odd/even}}^{M} \langle \hat{n}_i \rangle$; the imbalance is a commonly considered variable in the context of many-body localization in cold atoms [47]. In Fig. 5 we show both the local density on the central lattice site and the system imbalance. We also analyze the robustness of both quantities in the presence of dephasing. In the absence of this source of dissipation, both quantities allow us to differentiate between bosonic and fermionic dynamics as the profiles are significantly separated. However, while the differences in the local densities decrease at longer times, the fermionic imbalance exhibits much larger oscillations than the bosonic one, and this feature persists over the simulated length of time. We observe that the inclusion of dephasing, corresponding to the values shown in Figs. 5(b) and 5(d), reduces this clear separation. Nevertheless, this reduction is much stronger in the local density, whereas the even-odd imbalance seems to be more robust to the presence of dephasing.

Finally, in Fig. 6 we investigate whether this imbalance discrepancy remains robust in the presence of off-site interactions. As the imbalance is a highly oscillating function specially for the fermionic case, we present here a time-block averaged imbalance $\bar{\mathcal{I}} = \sum_i^{i+N_{\delta t}} |\mathcal{I}(t_i)|/N_{\delta t}$, where $N_{\delta t}$ is the number of time points over which we average. For the sake of clarity, the absolute value is required because the imbalance should

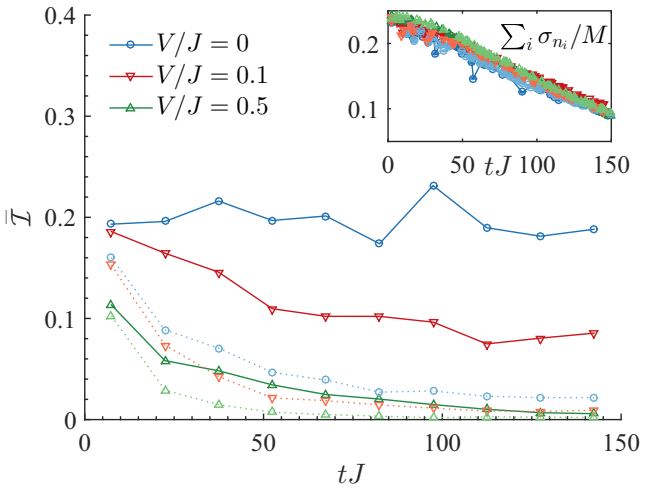

FIG. 6. Comparison of bosonic (dashed line) and fermionic (solid line) evolution of the time-block averaged imbalance $\bar{\mathcal{I}} = \sum_i^{i+N_{\delta t}} |\mathcal{I}(t_i)|/N_{\delta t}$ for a system with $M = 16$, $n_0 = 0.5$, $J = 1$, $dt = 0.001$, $N_{\delta t} = 300$, $\gamma_l = 0.01$, $\gamma_d = 0$, and variable off-site interaction strength V. The imbalance average drops over time in the presence of interaction but remain distinguishable for both species. Inset: Total density fluctuation for the same parameters, included for the purpose of comparison. Here all lines overlap while we observe relevant differences in the imbalance. These calculations are performed beginning from a charge density wave at half-filling, with a particle on each odd-numbered site.

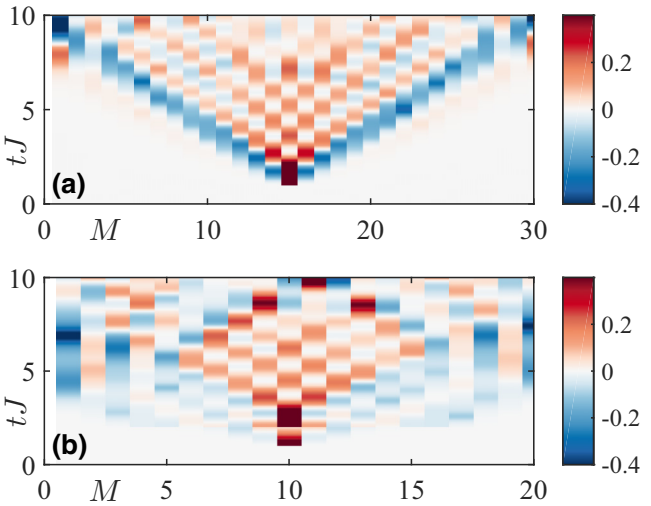

FIG. 7. (a) Evolution of the difference in density distribution Δn_i for a system with $M = 30$, $n_0 = 0.5$, $D = 128$, $dt = 0.001$, $J = 1$, $\tau_0 = 1$, $\delta_M = 0$. (b) Same as (a) for a system with $M = 20$ with no loss at $t = 0$, a first loss is induced at $t = \tau_0 = 1$ and a second loss occurs at $t = \tau_1 = 2\tau_0$. In contrast with the case of the first loss chosen at $t = 0$, differences between bosons and fermions are observed from the first loss event.

average to zero after a transient time much shorter than the timescale we simulate. Note again that the regime $V/J = 0.5$ could be accessible through dipole-dipole interactions, including interaction values up to $V \approx J$ and still compatible with HCBs.

We observe that as the interaction ramps up, the separation reduces between the fermionic and bosonic case. Nevertheless, the separation is still much greater than the one we can observe from the total fluctuations of the density. From this analysis we can establish that the imbalance—a global quantity related to local densities—is robust to moderate interactions and to moderate dephasing at rates comparable to the losses, and provides an interesting quantity with which to investigate differences between HCBs and spinless fermions also in the case of randomized losses in space and time.

VII. SUMMARY AND OUTLOOK

In this article, we have investigated how quantities that are related to the local density, and are experimentally measurable in quantum gas microscopes, allow us to distinguish between spinless fermions and hard-core bosons in the presence of particle loss. In the absence of loss, these quantities would in each case be identical for fermions and bosons. We have shown that the understanding of loss is not only a relevant element towards the correct description of the experimental conditions, but it can also play an essential role as a tool to access information about aspects of the closed-system dynamics.

In the future, understanding these processes could help probe particular types of many-body effects. It is an important ingredient to better understand the effects of losses in optical lattice experiments, as well as to investigate the effects of losses in the study of systems with slow intrinsic timescales, e.g., many-body localized states in the presence of dissipation.

ACKNOWLEDGMENTS

We thank A. Buyskikh, J. Surace, and J. Schachenmayer for helpful discussions. Work at the University of Strathclyde was supported by the EPSRC Programme Grant DesOEQ (EP/P009565/1), by the European Union Horizon 2020 collaborative project QuProCS–Quantum Probes for Complex Systems (Grant Agreement 641277), and by the EOARD via AFOSR grant number FA2386-14-1-5003. Results were obtained using the EPSRC-funded ARCHIE-WeSt High Performance Computer, EPSRC Grant No. EP/K000586/1.

APPENDIX A: LATTICE SIZE DEPENDENCE AND PRELOSS EVOLUTION DEPENDENCE IN HALF-FILLING

In Sec. V we studied the effects of deterministic losses in the distinction of fermionic and bosonic dynamics. However, we did not directly address the role of the boundaries in the differences discussed. In the case of unit filling, all the dynamics occur in a light cone of correlations generated by the ballistic motion of the hole, and so we are certain that the boundaries could not impact the densities in the center of the lattice for the time discussed $tJ \leqslant 10$. On the other hand, at half-filling, dynamics from $tJ = 0$ are affected by boundary effects, and so they could impact these dynamics. In Fig. 7(a) we analyze the density evolution for a system with $M = 30$ and half-filling, observing that the conelike spreading of the difference remains unperturbed by the boundaries for the simulated times. We can compare this result with Fig. 2(b) where we observe again the well-defined cone and results for $M = 20$

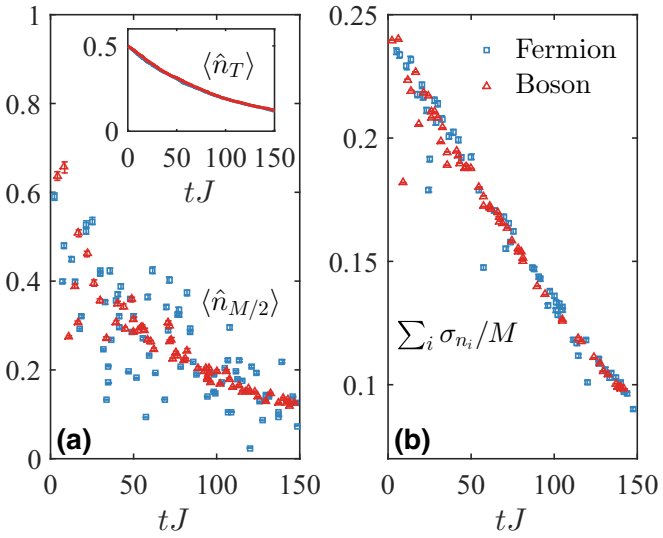

FIG. 8. (a) Comparison of bosonic and fermionic evolution of the middle site density $\langle \hat{n}_{M/2} \rangle$ for a system with $M = 16$, $n_0 = 0.5$, $J = 1$, $\gamma_l = 0.01$, $\gamma_d = 0$; numerical parameters are $dt = 0.001$ and $D = 200$. The inset shows the total particle number $\langle \hat{n}_T \rangle$ to provide some guidance over the evolution of the total occupation in the lattice as losses occur. (b) Same as (a) for the normalized total density fluctuations $\sum_i \sigma_{n_i}/M$. These calculations are performed beginning from a charge density wave at half-filling, with a particle on each even-numbered site. Note that these functions are rapidly oscillating, and that each point represents a snapshot of the values on a randomly spaced grid in time. The data include statistical error bars, which are contained within the point markers in most of the cases.

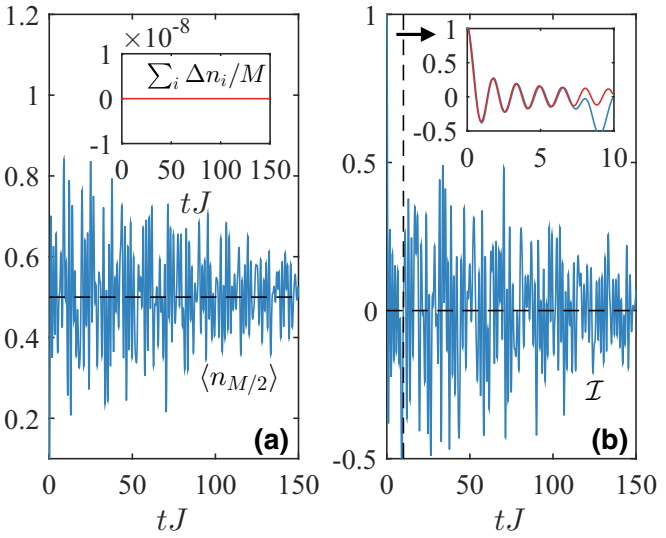

FIG. 9. (a) Closed system evolution of the middle site density $\langle \hat{n}_{M/2} \rangle$ for a system with $M = 16$, $n_0 = 0.5$, $J = 1$, $\gamma_l = 0$, $\gamma_d = 0$; numerical parameters are $dt = 0.001$ and $D = 150$. In the absence of loss both fermionic and bosonic results are identical, fluctuating around n_0. Inset: Averaged density difference between fermions and bosons; as predicted this quantity is zero. (b) Same as (a) for the imbalance $\mathcal{I}$. Again, fermions and bosons show the same profile, fluctuating around zero as expected for a nondisordered system. Inset: Short-time imbalance (blue) compared with the analytic result (red) that can be derived for free fermions. Note that the disagreement occurs at time $\sim M/2J$ that corresponds to the required time by an excitation to travel through the whole lattice, which is a finite-size effect.

and $M = 30$ coincide for times $tJ \lesssim 5$. After this time, the correlations associated with the first loss reach the boundary for $M = 20$, and we observe some resulting differences in the correlations. However, the main point remains unchanged, as we observe differences of the same magnitude between fermionic and bosonic dynamics even after the correlations hit the boundary.

Another point that was not directly addressed in the discussion was the possible impact of dynamics prior to the first loss event. This could only affect the case of half-filling as the initial state of the system is not an eigenstate of $\hat{H}$. In Fig. 7(b) we consider deterministic losses occurring at time $t = \tau_0$ and $t = \tau_1 > \tau_0$. As expected, due to the fact that the state at which the first loss occur does not have a unique particle number to the left anymore, the first loss will already affect differently fermions and bosons. Beyond some quantitative differences with the results in Figs. 2(b) and 2(d), we do not find relevant features in the profiles that indicate that the dynamics before the loss could enhance or reduce the distinction between bosons and fermions.

APPENDIX B: ROBUSTNESS IN AN EXPERIMENTAL MEASUREMENT SCHEME

In Sec. VI we discussed differences between fermionic and bosonic dynamics in the stochastic framework. It is important to note that the quantities studied in this section exhibit large fluctuations over time. As a result, it is important to consider how relevant it is to have access to full-time resolution to distinguish between particle statistics. In order to check whether these features are robust with limited time resolution in the experiments, we plot the evolution as a selection of snapshots in a random time grid. Note that Fig. 8 is generated from the same data set that we used in Fig. 4. Some features cannot be captured in this random grid such as the fact that both bosons and fermions overlap at short times since no loss has occurred on average. Nevertheless, we observe that there is still a clear distinction between fermions and bosons even after applying the grid. Note that we can observe the short-time drops in the density fluctuations [see Fig. 4(b)], which occur much more strongly for fermions as points that are outside the fluctuation profile. Consequently, we consider that the differences discussed would be robust in the realistic experimental conditions.

APPENDIX C: CLOSED SYSTEM DYNAMICS AND STOCHASTIC LOSSES

In Sec. VI we discussed differences in the local densities, density fluctuations, and imbalance profiles in the presence of losses. As background material we include here in Fig. 9 the evolution of the density in the middle site of the lattice and the imbalance, both in the absence of dissipation. Note that this evolution should coincide for bosons and fermions within the numerical error based on the discussion in Sec. III as the distinction between bosons and fermions arises from the

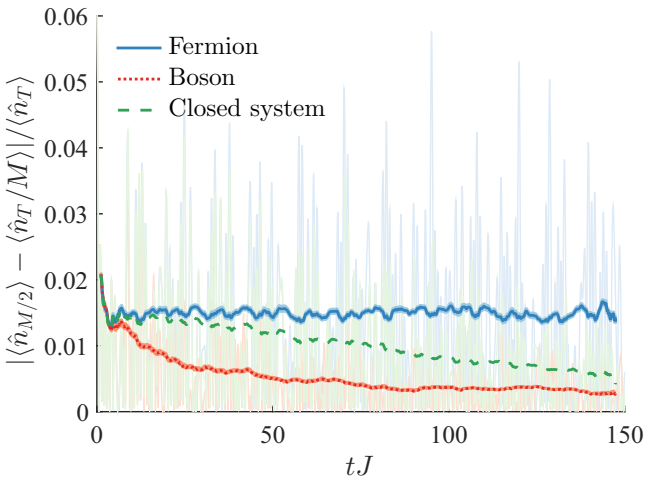

FIG. 10. Evolution of the middle site density fluctuation from the expected long-time average $|\langle\hat{n}_{M/2}\rangle - \langle\hat{n}_T/M\rangle|/\langle\hat{n}_T\rangle$ for a system with $M = 16$, $n_0 = 0.5$, $J = 1$, $\gamma_l = 0.01$, $\gamma_d = 0$, and a closed system ($\gamma_l = 0$). We provide time-block averages (lines) of the full data set (shades) for better visualization. We observe how the fermionic deviation remains approximately constant for the studied time, while the bosons and the closed system approach the long-time expected average with the former exhibits smaller deviations.

presence of particle losses in the dynamics. Our results agree with this statement as both quantities are identical for bosons and fermions [see inset of Fig. 9(a)].

In addition, we observe that in the closed system scenario the densities exhibit fluctuations in time around the average density $n_0 = n_T/M$ that decrease in amplitude slowly over time and remain relevant for the timescales discussed in Sec. VI. As they do not decay quickly in time compared to the typical loss timescale, we expect these fluctuations to be affected by losses in a different manner for different particle statistics. We also expect, even in the presence of losses, that the densities will average to the same value $n_0 = n_T(t)/M$ since the losses are homogenous in space. In Fig. 10 we compare the normalized density fluctuation from the predicted average density $|\langle\hat{n}_{M/2}\rangle - \langle\hat{n}_T/M\rangle|/\langle\hat{n}_T\rangle$ for closed, fermionic, and bosonic systems. In the closed system case, as we mentioned, the densities fluctuates around the average density per site $\langle\hat{n}_T/M\rangle$ with decreasing amplitude over time. However, we observe how the presence of loss preserves the fermionic fluctuations over time even beyond the closed system scenario, causing the opposite effect for bosons where the amplitude of fluctuations rapidly decreases around the predicted value. As these fluctuations overlap quite strongly for the three cases in Fig. 10, we also provide time-block averages (solid lines) to help visualizing how the fermionic fluctuations persist over time in comparison with bosons and the case of no losses.

Regarding the imbalance [Fig. 9(b)] we observe again long-lived fluctuations around the expected value of $\mathcal{I} = 0$ in the closed system. This result can be compared with Fig. 5(c) where again we observe how fermions show much higher fluctuations in time than the bosons. Another interesting point is that for short times, the imbalance can be computed analytically from mean field (see Ref. [48]) with it being proportional to $\mathcal{I} \propto J_0(4Jt)$ where J_0 denotes the zeroth-order Bessel function. Our finite-size calculations agree with the analytical result up to times of the order of $t \sim M/2J$.

[1] I. Bloch, J. Dalibard, and S. Nascimbene, Nat. Phys. **8**, 267 (2012).

[2] M. Lewenstein, A. Sanpera, and V. Ahufinger, *Ultracold Atoms in Optical Lattices: Simulating Quantum Many-Body Systems* (Oxford University Press, Oxford, 2012).

[3] H. Pichler, A. J. Daley, and P. Zoller, Phys. Rev. A **82**, 063605 (2010).

[4] S. Sarkar, S. Langer, J. Schachenmayer, and A. J. Daley, Phys. Rev. A **90**, 023618 (2014).

[5] P. Barmettler and C. Kollath, Phys. Rev. A **84**, 041606 (2011).

[6] M. Müller, S. Diehl, G. Pupillo, and P. Zoller, Adv. Atomic Mol. Opt. Phys. **61**, 1 (2012).

[7] I. Vidanović, D. Cocks, and W. Hofstetter, Phys. Rev. A **89**, 053614 (2014).

[8] G. Kordas, S. Wimberger, and D. Witthaut, EPL (Europhys. Lett.) **100**, 30007 (2012).

[9] H. P. Lüschen, P. Bordia, S. S. Hodgman, M. Schreiber, S. Sarkar, A. J. Daley, M. H. Fischer, E. Altman, I. Bloch, and U. Schneider, Phys. Rev. X **7**, 011034 (2017).

[10] M. V. Medvedyeva, T. Prosen, and M. Žnidarič, Phys. Rev. B **93**, 094205 (2016).

[11] E. Levi, M. Heyl, I. Lesanovsky, and J. P. Garrahan, Phys. Rev. Lett. **116**, 237203 (2016).

[12] M. H. Fischer, M. Maksymenko, and E. Altman, Phys. Rev. Lett. **116**, 160401 (2016).

[13] E. P. van Nieuwenburg, J. Y. Malo, A. J. Daley, and M. H. Fischer Quantum Science and Technology **3**, 1 (2017).

[14] M. Girardeau, J. Math. Phys. **1**, 516 (1960).

[15] T. Kinoshita, T. Wenger, and D. S. Weiss, Science **305**, 1125 (2004).

[16] T. Stöferle, H. Moritz, C. Schori, M. Köhl, and T. Esslinger, Phys. Rev. Lett. **92**, 130403 (2004).

[17] B. Paredes, A. Widera, V. Murg, O. Mandel, S. Folling, I. Cirac, G. V. Shlyapnikov, T. W. Hansch, and I. Bloch, Nature (London) **429**, 277 (2004).

[18] P. M. Preiss, R. Ma, M. E. Tai, A. Lukin, M. Rispoli, P. Zupancic, Y. Lahini, R. Islam, and M. Greiner, Science **347**, 1229 (2015).

[19] S. Sachdev, *Quantum Phase Transitions* (Cambridge University Press, Cambridge, 2001).

[20] M. Boll, T. A. Hilker, G. Salomon, A. Omran, J. Nespolo, L. Pollet, I. Bloch, and C. Gross, Science **353**, 1257 (2016).

[21] M. F. Parsons, A. Mazurenko, C. S. Chiu, G. Ji, D. Greif, and M. Greiner, Science **353**, 1253 (2016).

[22] L. W. Cheuk, M. A. Nichols, K. R. Lawrence, M. Okan, H. Zhang, E. Khatami, N. Trivedi, T. Paiva, M. Rigol, and M. W. Zwierlein, Science **353**, 1260 (2016).

[23] P. T. Brown, D. Mitra, E. Guardado-Sanchez, P. Schauß, S. S. Kondov, E. Khatami, T. Paiva, N. Trivedi, D. A. Huse, and W. S. Bakr, Science **357**, 1385 (2017).

[24] E. Haller, J. Hudson, A. Kelly, D. A. Cotta, B. Peaudecerf, G. D. Bruce, and S. Kuhr, Nat. Phys. **11**, 738 (2015).
[25] G. J. A. Edge, R. Anderson, D. Jervis, D. C. McKay, R. Day, S. Trotzky, and J. H. Thywissen, Phys. Rev. A **92**, 063406 (2015).
[26] R. Dum, A. S. Parkins, P. Zoller, and C. W. Gardiner, Phys. Rev. A **46**, 4382 (1992).
[27] K. Mølmer, Y. Castin, and J. Dalibard, J. Opt. Soc. Am. B **10**, 524 (1993).
[28] A. J. Daley, Adv. Phys. **63**, 77 (2014).
[29] D. C. McKay and B. DeMarco, Rep. Prog. Phys. **74**, 054401 (2011).
[30] C. Weitenberg, M. Endres, J. F. Sherson, M. Cheneau, P. Schausz, T. Fukuhara, I. Bloch, and S. Kuhr, Nature (London) **471**, 319 (2011).
[31] T. Gericke, P. Wurtz, D. Reitz, T. Langen, and H. Ott, Nat. Phys. **4**, 949 (2008).
[32] H. A. Gersch and G. C. Knollman, Phys. Rev. **129**, 959 (1963).
[33] D. Poletti, P. Barmettler, A. Georges, and C. Kollath, Phys. Rev. Lett. **111**, 195301 (2013).
[34] S. R. White, Phys. Rev. Lett. **69**, 2863 (1992).
[35] F. Verstraete, V. Murg, and J. I. Cirac, Adv. Phys. **57**, 143 (2008).
[36] U. Schollwöck, Ann. Phys. **326**, 96 (2011).
[37] G. Vidal, Phys. Rev. Lett. **91**, 147902 (2003).
[38] B. Pirvu, V. Murg, J. I. Cirac, and F. Verstraete, New J. Phys. **12**, 025012 (2010).
[39] F. Verstraete, J. J. García-Ripoll, and J. I. Cirac, Phys. Rev. Lett. **93**, 207204 (2004).
[40] U. Schollwöck, Rev. Mod. Phys. **77**, 259 (2005).
[41] A. J. Daley, C. Kollath, U. Schollwöck, and G. Vidal, J. Stat. Mech. (2004) P04005.
[42] E. Lieb and D. Robinson, Commun. Math. Phys. **28**, 251 (1972).
[43] R. Islam, R. Ma, P. M. Preiss, M. Eric Tai, A. Lukin, M. Rispoli, and M. Greiner, Nature (London) **528**, 77 (2015).
[44] A. J. Daley, H. Pichler, J. Schachenmayer, and P. Zoller, Phys. Rev. Lett. **109**, 020505 (2012).
[45] H. Pichler, L. Bonnes, A. J. Daley, A. M. Läuchli, and P. Zoller, New J. Phys. **15**, 063003 (2013).
[46] A. Frisch, M. Mark, K. Aikawa, S. Baier, R. Grimm, A. Petrov, S. Kotochigova, G. Quéméner, M. Lepers, O. Dulieu *et al.*, Phys. Rev. Lett. **115**, 203201 (2015).
[47] M. Schreiber, S. S. Hodgman, P. Bordia, H. P. Lüschen, M. H. Fischer, R. Vosk, E. Altman, U. Schneider, and I. Bloch, Science **349**, 842 (2015).
[48] P. Barmettler, M. Punk, V. Gritsev, E. Demler, and E. Altman, Phys. Rev. Lett. **102**, 130603 (2009).